RTTOV-10
SCIENCE AND VALIDATION REPORT

**Roger Saunders[1], James Hocking[1], Peter Rayer[1],
Marco Matricardi[2], Alan Geer[2], Niels Bormann[2],
Pascal Brunel[3], Fatima Karbou[3] and Filipe Aires[4]**

Affiliations:
[1]Met Office, U.K.
[2]European Centre for Medium Range Weather Forecasts
[3]MétéoFrance
[4]Estellus, France

Change record			
Version	Date	Author / changed by	Remarks
0.1	14 Oct 10	R W Saunders	First draft version requesting input from partners
0.2	22 Nov 10	R W Saunders	Added text from various contributors
0.3	20 Dec 10	R W Saunders	More contributions added
0.4	28 Oct 11	R W Saunders	Ditto
0.5	14 Nov 11	R W Saunders	Final draft after all comments
1.0	16 Nov 11	R W Saunders	Draft for release
1.1	20 Dec 11	R W Saunders	Improved IR cloudy simulation text
1.11	23 Jan 12	R W Saunders	Updated secs 2.2/4.7 on FASTEM

Table of contents

1.   Introduction and Documentation

The purpose of this report is to document the scientific aspects of the latest version of the NWP SAF fast radiative transfer model, referred to hereafter as RTTOV-10, which are different from the previous model RTTOV-93 and present the results of the validation tests which have been carried out. The enhancements to this version, released in Jan 2011, have been made as part of the activities of the EUMETSAT NWP-SAF. The RTTOV-10 software is available at no charge to users on request from the NWP SAF web site. The licence agreement to complete is on the NWP SAF web site at: http://research.metoffice.gov.uk/research/interproj/nwpsaf/request_forms/ . The RTTOV-10 documentation, including the latest version of this document can be viewed on the NWP SAF web site at: http://research.metoffice.gov.uk/research/interproj/nwpsaf/rtm/ which may be updated from time to time. Technical documentation about the software and how to run it can be found in the RTTOV-10 user's guide which can be downloaded from the link above and is provided as part of the distribution file to users.

The baseline document for the original version of RTTOV is available from ECWMF as Eyre (1991) and the basis of the original model is described in Eyre and Woolf (1988). This was updated for RTTOV-5 (Saunders *et. al.* 1999a, Saunders *et. al.,* 1999b) and for RTTOV-6, RTTOV-7, RTTOV-8 and RTTOV-9 (Matricardi *et. al.,* 2004) with the respective science and validation reports for each version hereafter referred to as R7REP2002, R8REP2006, R9REP2008 respectively all available from the NWP SAF web site at the link above. The changes described here only relate to the scientific differences from RTTOV-93. For details on the technical changes to the software, user interface etc. the reader is referred to the RTTOV-10 user manual available from the RTTOV-10 web page at: http://research.metoffice.gov.uk/research/interproj/nwpsaf/rtm/rtm_rttov10.html .

This document also describes comparisons and validations of the output values from this new version of the model by comparing with previous versions, other models and observations. Only aspects related to new and improved science are presented in this report. Many of the details of the science and validation are given in other reports which are referenced in this document and so only a summary is presented here in order to keep this document manageable in size.

2.   Scientific Changes from RTTOV-9 to RTTOV-10

The main scientific changes from RTTOV-9 to RTTOV-10 are described below in detail. In summary they are:

- − Infrared and Microwave land surface emissivity atlases included as an option for improved simulations of window channels over land

- − Improved Microwave emissivities over ocean using FASTEM-4

- − Computation of principal components of radiances for IASI and AIRS

- − Cloud water concentrations can now be given for any combination of cloud types in each layer

- − Inclusion of explicit treatment of the Zeeman effect for AMSU-A channel 14 and SSMIS channels 19-22.

- Improvements to treatment of top layer of user input profile

- Updated IR sensor coefficients based on latest spectroscopy using LBLRTMv11

- Updated MW sensor coefficients with improved atmospheric layering

- The number of layers for the optical depth calculation has increased from 43 to 50 for IR and MW radiometers

- Updated SSU coefficients based on latest spectroscopy LBLRTMv11

- Improvements to microwave scattering code

In addition the code was rewritten to use more of the Fortran-90 structures. More details of each scientific change are given below.

2.1   Land surface emissivity atlases

2.1.1   Infrared emissivity atlas

To improve simulations of infrared window channel radiances over land an atlas has been created to provide an estimated mean and variance of the land surface emissivity at high spectral resolution for input to RTTOV-10. For RTTOV-9 and earlier versions the calculations of upwelling infrared radiances over land are reliant on a single emissivity value, assumed to be a constant of 0.98 for all wavelengths. Recently an infrared emissivity atlas (http://cimss.ssec.wisc.edu/iremis) and high spectral resolution emissivity algorithm based on MODIS and laboratory measurements have been developed by Seemann et al. (2008) and Borbas et al. (2007). They have been shown to provide more accurate simulations of SEVIRI radiances (Koenig and de Coning; 2009) over land. The theory of the creation of the RTTOV-10 IR land surface emissivity module and its evaluation with SEVIRI and IASI observations and its assessment in assimilation mode are all documented in Borbas et. al. (2011). Some examples of the improved simulations obtained using this atlas are also given in section 4.3.

2.1.2   Microwave emissivity atlases

Simulations of microwave window channels would also benefit from a more accurate first guess emissivity and associated error covariance. The TELSEM module is an innovative emissivity interpolator that provides an emissivity estimate for each location over the continents and each month of the year (Prigent et al. 2008). It is a general and flexible tool allowing for changing emissivity frequencies, view angle and channel polarisation. TELSEM has been developed as part of RTTOV-10. It is based on an emissivity climatology from more than 15 years of SSM/I observations (emissivities have been derived from satellite observations by suppressing the atmospheric contribution following the methodology initiated by Prigent et al. 1997; 2006). As a consequence, TELSEM was originally designed to provide land surface emissivities for frequencies between 19 and 85 GHz. However, it can be used for lower or higher frequencies. Tests based on AMSU-A, AMSR-E, HSB, and MHS observations have shown that it works down to 6 GHz and up to 190GHz (Aires et al. 2011). The emissivities computed by TELSEM can be improved using a physical retrieval scheme. The details of the TELSEM land surface microwave emissivity model and its validation are described in Aires et. al. (2011).

2.1.3   *Alternative microwave emissivity atlas for AMSU-A and -B*

As an alternative to the TELSEM module an atlas containing one year of emissivity estimates as monthly means at 23, 31, 50 and 89GHz, is also available for use in RTTOV-10. The land surface emissivity is directly retrieved in AMSU window channels using observed brightness temperatures (for 2009) by removing the effects of rain, clouds and atmosphere (Karbou et al. 2006). The atmospheric contribution to the measured signal is estimated using short-range forecast fields. For each month, mean emissivity estimates, together with their standard deviations, are provided at four frequencies and at two observation zenith angles: angles greater than 40 deg and those lower than 40 deg. This is important to account for the angular dependence of the surface emissivity. The emissivity estimates were found very useful for improving RTTOV simulations for AMSU-A and AMSU-B window and sounding channels (Karbou et al. 2010). This atlas from CNRM can be downloaded from the RTTOV-10 web page.

2.2   *A new ocean surface emissivity model FASTEM-4/5*

The fast microwave emissivity model (FASTEM) has been widely utilized to compute the surface emitted microwave radiation over the ocean. However this model was developed for frequencies in the range 20-60 GHz and is biased at higher and lower frequencies. Several components such as variable sea surface salinity and a full Stokes vector have not been generally taken into account in earlier versions of FASTEM. A new version of FASTEM has been developed for RTTOV-10 (FASTEM-4) where a new permittivity model is generated by using the measurements for fresh and salt water at frequencies between 1.4 GHz and 410 GHz. A modified sea surface roughness model from Durden and Vesecky (1985) is applied to the two-scale surface emissivity calculations and the treatment of foam has been updated. The capability for simulating polarimetric sensors has also been improved. This microwave ocean emissivity model (also called OEMM) is now being used in the Community Radiative Transfer Model (CRTM) and has resulted in some improvements in microwave radiance simulations. More details of the FASTEM-4 model and its validation are given in Liu et. al. (2010) and some validation of the model in the ECMWF IFS system is presented in Bormann *et. al.* (2011) and in section 4.7.

After the release of RTTOV-10.1 some problems were seen with simulations of AMSU-A radiances (with the possible exception of channel 1), where the FASTEM-4 distribution had a larger dependence on wind-speed than previous versions of FASTEM. This is mostly seen in the slope of the histogram peak for wind-speeds less than 10m/s, but is also noticeable in the very small number of observations with wind-speeds greater than 20m/s. The problem was tracked down to the new foam model and the fitting model for the large scale part of the correction. As a result the FASTEM model was updated to v5 for the delta release of RTTOV (v10.2) where the foam model was reverted to that used in FASTEM-3 and an improved fitting to the large scale correction was implemented. The small scale correction in FASTEM-4 is retained in FASTEM-5.

2.3   *The computation of principal components for IASI and AIRS*

For the advanced infrared IR sounders (e.g. AIRS and IASI) an enhancement of the RTTOV model has been developed that exploits principal component analysis. The model is based on the computation of a database of line-by-line spectra for a large training set of diverse atmospheric situations. The principal component scores obtained from the eigenvectors of the covariance matrix of the simulated radiances are used in a linear regression scheme where they are expressed as a linear combination of profile dependent predictors. The predictors consist of a selected number of polychromatic radiances computed using the standard RTTOV fast transmittance model. The linear regression scheme can then be used to simulate principal component scores and consequently reconstruct radiances for any input atmospheric profile. The principal component based model is similar to the conventional RTTOV model in terms of speed and the dimensionality reduction inherent in the use of principal component analysis makes the principal component based RTTOV much more computationally efficient for sensors with many channels. Because of the highly linear relationship between the principal component scores and the independent variables used in the regression scheme, the principal component based RTTOV can reproduce the underlying line-by-line radiances to a higher degree of accuracy. In addition to the improvements in accuracy and computational efficiency, the availability of a principal component based fast radiative transfer will enable the RTTOV user to exploit the noise reduction capability of principal component analysis and allow investigation of the direct assimilation of IASI principal component scores for instance in spectral regions affected by high instrument noise. The details of the principal component implementation in RTTOV-10 are described in Matricardi (2010a) and Matricardi (2010b).

2.4   *Inclusion of more than one cloud type within a layer for cloudy IR simulations*

RTTOV treats the problem of radiative transfer in the presence of multiple layers partly covered by clouds using a multi-stream method that divides the atmosphere into a number of homogeneous columns (Matricardi, 2005). Each column contains either cloud-free layers or totally cloudy layers and the top of the atmosphere radiance is written as the sum of radiances from each column weighted by the column area coverage. The total number of columns depends on the number of cloudy layers and the cloud fraction in each of these layers. Depending on the cloud distribution, the stream model can result in a clear stream of a given weight for which clear sky radiances are computed. In the context of the stream model, the clear sky radiance can include the effect of aerosols. In previous versions of RTTOV (i.e. RTTOV-9), the user could define a mixture of cloud and aerosols particles in each layer but was not allowed to place two different cloud types on the same layer (i.e. it was not possible to compute the optical properties for a combination of different cloud particles, for instance a combination of water droplets and ice crystals). In RTTOV-10 this limitation has been removed and in each of the RTTOV layers the user can now define any combination of scattering particles. It should be noted that results are based on the approximation that scattering particles in the layer do not interact with each other (i.e. the optical properties for a combination of scattering particles is the sum of the optical properties of the single particles). The user should also note the limitation that when more than one cloud type is placed in the layer, the specification of the cloud fraction in the layer

can only be specified for all the cloud in the layer not for each individual cloud type. The RTTOV-10 user guide has more details of what to specify in the arrays.

2.5 Inclusion of Zeeman Effect

An option for RTTOV-10 is provided, based on a scheme developed by Han (2007), to include the Zeeman effect for high peaking MW channels. Coefficients for this were derived for an augmented set of optical depth predictors for channels 19-22 of SSMIS and for channel 14 of AMSU-A. This implementation was ultimately based on line by line transmittances calculated with the Rosenkranz-88 model (Rosenkranz and Staelin 1988) for a dependent set of 48 diverse profiles from UMBC, and imported into RTTOV.

For AMSU-A, the effect on the brightness temperatures is small (up to 0.5K), but for the SSMIS mesospheric channels it is large (up to 10 K). In both cases the impact varies with the magnetic field strength, with the angle between the magnetic field and the viewing path to the instrument, and with the proximity of oxygen lines to the instrument channels. The magnetic field range used in the training set for the coefficients was restricted to 20-70 µT. For inclusion within RTTOV-10, no scientific changes were made to the method developed by Han (2007). The new SSMIS coefficients which include the Zeeman effect use 83 levels from 0.0002 hPa to 1013.25 hPa.

In RTTOV-10, the radiative transfer integration, which is on user levels, incorporates predicted optical depths to space from all levels, including the top of atmosphere (in RTTOV-9 the topmost value is assumed to be zero). The optical depths will have been interpolated from the extended pressure grid used by the Zeeman coefficients to the user's pressure grid, and if this leaves many absorbing layers above its topmost level, a likely case for SSMIS channel 20, then the value interpolated to this level may be significantly greater than zero. This means that, although no thermal emission will be calculated for the gas above the user's top level, some account will have already been taken of the absorption. To remedy this inconsistency, an option is included to set the topmost optical depths to zero in all channels directly after the interpolation. If the user's top of atmosphere is at 0.005 hPa, say, then taking this option will have no significant effect except for channels with sensitivity extending into the mesosphere.

2.6 Refinements in the Line-by-Line transmittance databases and layering for coefficient generation

2.6.1 New atmospheric layers for IR and MW coefficients

For previous versions of RTTOV the coefficients for radiometers were provided on 43 levels. It became evident from user feedback that these levels were not optimal for several reasons:
- There were not enough levels to cover the stratosphere which degraded AMSU-A stratospheric channel simulations
- The lowest level was at 1013 hPa which meant many profiles had to be extrapolated in high pressure situations.
- A fixed 'hidden' top level, not specified in the user profile, made the top layer isothermal, and led to significant errors in high peaking IASI channels.

As a result the optimal number of levels for IR and MW radiometers was reviewed. The basis for this review, providing an ensemble of atmospheres, was the 'reduced' set of 52 profiles constructed by ECMWF to capture the statistical envelope of a set of 13495 model-based profiles, originally on 60 levels. For this reduced set, which supplied the training profiles for RTTOV-9 coefficients, values of temperature and gas abundance are available on the AIRS 101 level pressure grid and, by interpolation, on the 44 level grid used for RTTOV-9 – 43 levels plus the top of atmosphere at 0.005 hPa.

An 'ideal' set of 60 levels was first constructed by interleaving all the upper levels (above 5 hPa) from the 101 level pressure grid with those on 44 levels, followed by a set of 'less-than-ideal' grids using an intermediate number of levels. These grids, there were nine, all included a level at 0.01 hPa to reduce the depth of the top layer and to allow for a later upgrade of the Zeeman implementation for AMSU-A. To improve the representation at the surface the grid chosen has the level at 1013.25 hPa replaced with two levels at 1025.0 hPa and 1050.0 hPa.

101L (hPa)	51L (hPa)	44L (hPa)
0.0050	0.005	0.005
0.0161	0.01	
0.0384		
0.0769		
	0.10	0.10
0.1370		
0.2244	0.20	
		0.29
0.3454		
0.5064	0.50	
		0.69
0.7140	0.80	
0.9753		
1.2972	1.20	
		1.42
1.6872	1.60	
2.1526	2.20	
		2.61
2.7009	2.70	
3.3398	3.50	
4.0770	4.20	
		4.41
4.9204	5.00	
5.8776		
6.9567	6.95	6.95
101L	**51L**	**44L**
986.0666		
	1005.43	1005.43
1013.9476		1013.25
	1025.00	
1042.2319		
	1050.00	
1070.9170		
1100.0000		

Table 1. The middle column shows (in hPa) the new pressure grid on 51 levels where it differs, at top and bottom, from the 44 level grid. For comparison, the AIRS 101 level grid is shown to its left and the original 44 level grid to its right.

Coefficient files were generated from the 52 profile set, appropriately interpolated, for these new pressure grids and the RTTOV-10 development code was used for AMSU-A to produce tables of brightness temperature departures from the 101 level results in the form of bias and RMSE over both the set of 13495 profiles (on 44 levels) and an independent 83 profile set (on 101 levels). From this data, after minor smoothing and fine tuning, the 51 level grid shown in Table 1 was chosen as the standard for RTTOV-10, embodying a trade-off between increased computation time with the extra levels and accuracy of the calculations.

The channel biases for the 83 profile test (101 level inputs) are set out in Table 2, and show a significant decrease for the stratospheric channels (11-14) in moving the coefficients from 44 levels to 51 levels, and the pattern is very similar for the corresponding channel root mean square differences, which are set out in Table 3. Coefficients on the 51 level grid give results that are closer to those from coefficients on the ideal 60 level grid for all channels, but this is most noticeable for those peaking in the stratosphere. For instance, the channel 14 RMSE with respect to the 101 level reference shows a five-fold decrease - from 0.63 K for 44 levels to 0.11 K for 51 levels.

Channel	101L-60L	101L-51L	101L-44L
1	-0.0574	-0.0469	-0.0574
2	-0.0267	-0.0190	-0.0267
3	0.0068	0.0183	0.0068
4	0.0003	0.0062	0.0010
5	-0.0239	-0.0227	-0.0221
6	-0.0407	-0.0411	-0.0382
7	-0.0383	-0.0361	-0.0376
8	-0.0253	-0.0240	-0.0257
9	0.0304	0.0294	0.0321
10	0.0634	0.0629	0.0711
11	0.1096	0.1067	0.1455
12	0.1345	0.1370	0.2963
13	0.0648	0.0815	0.4809
14	0.0032	0.0042	0.5118
15	-0.0635	-0.0483	-0.0635

Table 2. RTTOV brightness temperature differences for AMSU-A relative to 101L 83 profile set.

Channel	101L-60L	101L-51L	101L-44L
1	0.1515	0.1390	0.1515
2	0.1002	0.0927	0.1002
3	0.1205	0.1170	0.1205
4	0.0662	0.0655	0.0665
5	0.0367	0.0355	0.0352
6	0.0457	0.0459	0.0434
7	0.0454	0.0435	0.0447
8	0.0332	0.0323	0.0336
9	0.0577	0.0572	0.0578
10	0.0898	0.0892	0.0938
11	0.1337	0.1306	0.1638
12	0.1607	0.1614	0.3213
13	0.0774	0.0926	0.5254
14	0.0247	0.1063	0.6321
15	0.1784	0.1549	0.1784

Table 3. RTTOV brightness temperature differences for AMSU-A. RMSE difference relative to 101L for 83 profile set

2.6.2 Infrared transmittances

For all of the RTTOV-10 infrared coefficient files the LBLRTMv11.1 model developed at AER (Clough et al., 2005) has been used together with the MTCKD continuum absorption (mt_ckd_1.4). For the LBL computations a molecular database was created that blends line parameters obtained from different sources. This choice is based on the results shown in Matricardi (2007) which suggest that in a number of spectral regions the use of alternative line parameters can result in a better agreement between observations and simulations. One database is based on the AER file supplied with the LBLRTM_v11.1 package. This file is largely drawn from HITRAN2004 (Rothman et. al.; 2005) and includes updates up to January 2007. However, for the ozone region between 1000 and 1080 cm^{-1} ozone line parameters from HITRAN_2000 (Rothman et al.; 2003) are used whereas in the spectral region between 1700 and 2400 cm^{-1} water vapour line parameters from GEISA_2003 (Jacquinet-Husson et al.; 2005) are used. The diverse profile dataset used was the 83 diverse profile set from the 91L ECMWF analyses interpolated on to 51 levels for IR radiometers and 101 levels for advanced IR sounders (Chevallier et. al.; 2006).

2.6.3 Refinements to computation of microwave transmittances

The AMSUTRAN line-by-line model calculates channel-averaged transmittances to space for the RTTOV microwave sensors, with water vapour as the only variable gas, and with oxygen, nitrogen and ozone as the mixed gases. As for RTTOV-9, ozone is only included for channels near 183 GHz, where it exhibits a systematic decrease in brightness temperature of a few tenths of a degK.

The AMSUTRAN oxygen code is based on the Liebe MPM-93 Liebe (1993) code, but uses line parameters from MPM-92. A scalar approximation to the Zeeman effect in MPM-93 was found to be detrimental for AMSU-A (Kobayashi et. al, 2007) and its omission was reflected in updated coefficients after the release of RTTOV-9. An alternative scheme to include the Zeeman effect in RTTOV-10 is described in section 2.5, and two other changes recommended by Kobayashi et. al. (2007) were incorporated for RTTOV-10.

The first of these changes is an option to use the Curtis-Godson approximation, for the representation of layer variables. This is an improvement over the original average of the top and bottom layer boundary values, which will lead to an overestimation of the absorption for an optically thick layer. The new method replaces this with a density-weighted average over the layer, assuming an exponential distribution of pressure across the layer, and including a renormalization to conserve the number of molecules. The second change is a correction to the method of channel averaging over the band-pass. The outermost steps of the band-pass were originally the same width as the internal steps, whereas they should be half this width to preserve the band-pass.

Another change was to remove two hidden levels, the model-top and a level to split the input top layer, which were originally hard-wired into the code. With the release of RTTOV-10, *all* levels of an input profile must be provided externally, and AMSUTRAN has been modified to work in the same way.

2.6.4 New SSU coefficients

The Stratospheric Sounding Unit (SSU) is a three-channel infrared radiometer designed to measure radiances in the 15μm carbon dioxide absorption band. It uses a pressure modulation technique where the pressure in a cell of carbon dioxide gas in the instrument's optical path is varied in a cyclic manner. The spectral performance of the instrument depends on the mean cell pressure, whose long-term stability is crucial for obtaining time consistent observations. The cell pressures decrease after launch causing a change in the spectral response as shown in Kobayashi et. al. (2008) and Kobayashi et. al. (2009) who show typical changes to the weighting functions due to this effect.

Prior to RTTOV-10 the coefficients for SSU were based on a very old line-by-line model **tranh** developed at NESDIS in the early 1980s. Using the LBLRTMv11.3 line-by-line radiative transfer model (Clough et al., 2005) and the HITRAN line parameter database (Rothman et al., 2005) the transmittances and hence coefficients for all the SSU instruments were updated with the latest spectroscopy and to include CO_2 pressure as a variable using the v8 predictor set defined in R8REP2006. Data is available on the SSU cell pressures as a function of time. It is proposed to use this updated model for SSU simulations in the ERA-CLIM reanalysis.

3. Changes to the microwave scattering code for RTTOV-10

The microwave scattering code RTTOV-SCATT (Bauer *et. al.* 2006) has a separate interface from the rest of RTTOV. The changes listed here affect only the microwave scattering code itself - no changes affect the core of RTTOV.

The main scientific change for RTTOV-10 is a revised approach to cloud overlap, which gives a better fit to reference radiative transfer calculations and to observations. This facility was added as an option in RTTOV-9.3 but becomes the default for RTTOV-10. A second change with scientific impact is part of a package of performance enhancements. Most of these were purely technical, such as removing unnecessary initialisations and

copies. However, there was a small scientific impact from an optimisation of the number of atmospheric levels for which Eddington scattering radiative transfer is done.

3.1 *Cloud overlap*

At microwave frequencies, the nonlinear dependence of radiance on hydrometeor amount causes a 'beamfilling effect' in satellite observations, so that even when two fields of view contain the same mass of rain or cloud, variations in fractional cloudiness can cause large differences in measured radiances. For performance reasons, RTTOV-SCATT uses only two independent columns for radiative transfer: one with multiple scattering which contains any cloud or precipitation, and one that is purely clear sky. To approximate sub-grid cloud variability, the grid-box average brightness temperature T is computed from a weighted combination of cloudy and clear-sky parts:

$$T = (1 - C)T_{Clear} + CT_{Cloudy} \qquad (1)$$

The new overlap formulation (Geer et al. 2009a) finds a way of substantially improving the accuracy of this approximation by making a more appropriate choice for the value of C, the effective cloud fraction, in the grid box. Originally, it was set to the maximum cloud fraction in the atmospheric profile. However, this gave an excessive weighting to cloud and, through the beamfilling effect, caused substantial biases in the radiative transfer model. The new approach uses the profile-average cloud fraction, which is more representative of radiative transfer at microwave frequencies. It reduces rms errors by 40% in areas of rain or heavy cloud when 'truth' comes from multiple independent column simulations. There is improvement all the way from low (e.g. 19GHz) to high (e.g. 183GHz) microwave frequencies. There is also improvement when 'truth' comes from microwave imager observations.

RTTOV-10 also gives users the option to choose their own value for C (see User Guide). This means they can apply their own cloud overlap approach in the computation of C, which allows a standardisation of overlap approaches between the atmospheric model and the radiance operator in data assimilation systems (Geer et al. 2009b).

3.2 *Performance optimisation*

RTTOV-SCATT splits the vertical profile into two parts, with a lower part (starting from the surface) where significant scattering may occur and the Eddington solution to radiative transfer is applied, and one (starting from the top of the atmosphere) where no scattering computations are necessary and the integral solution to radiative transfer can be used. The Eddington is more computationally expensive so it is useful to limit the number of vertical levels involved.

In RTTOV-9, the top layer of the Eddington calculations was placed at the highest atmospheric level for which a single scattering albedo greater than 10^{-8} was found. This limit is controlled by the parameter *min_ssa* in rttov_const.F90. Brightness temperatures were

simulated for a near-global sample of 40,000 atmospheric profiles corresponding to 12hrs of SSM/I data assimilated at ECMWF. Various different values of *min_ssa* were tried and the results compared to a reference with *min_ssa* = 10^{-8}. Figure 1 shows the results for SSM/I channel 85h, which exhibited the largest differences of any SSM/I channel.
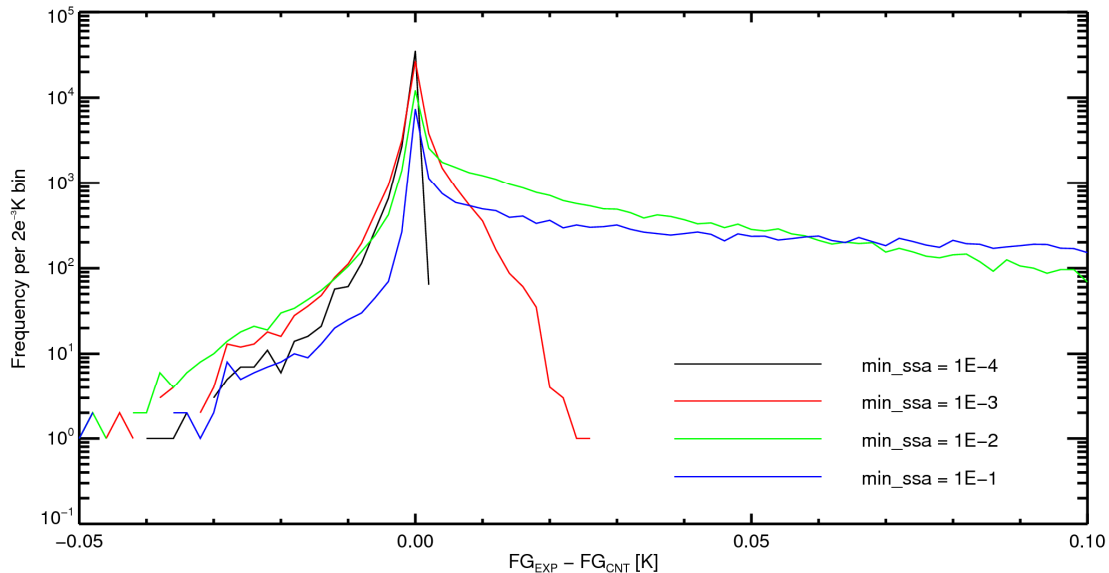

Figure 1: Logarithmic histograms of the discrepancy between brightness temperatures computed with more computationally efficient values of min_ssa and a reference (equivalent to RTTOV-9) with min_ssa = 10^{-8}. Based on a sample of 40,000 atmospheric profiles from the first guess (FG) of the ECMWF system. Simulations are for SSM/I channel 85h.

A value of *min_ssa* = 10^{-3} reduces the number of vertical levels used in the Eddington by an average of 40%, but only affects brightness temperature by a maximum of ±0.05K. Hence 10^{-3} was chosen as the new default. This makes a small contribution to a package of performance enhancements that overall reduces the cost of RTTOV-SCATT by about 30%.

4. Testing and Validation of RTTOV-10

To ensure no bugs have entered in the RTTOV code during the introduction of the above changes an extensive set of tests were applied to the new model before it was released to users. For example the use of the RTTOV-7 optical depth predictors should give identical results with the new code to the old RTTOV-9 code. There was also an extensive series of comparisons carried out, not described here, between RTTOV-9 and RTTOV-10 transmittances, radiances, jacobians and surface emissivities from the direct, TL, AD and K codes to check there are no differences during the code development except those anticipated. The tests conducted are in the RTTOV-10 test plan document and users can run these tests to verify the performance of the code on their platform when they first install RTTOV.

To ensure there are no significant unexpected changes from RTTOV-9 the new RTTOV-10 code is validated in several ways:

- The RTTOV-10 top of atmosphere radiances computed using the old (GENLN2, 43L) and new (LBLRTM, 51L) model transmittances from a 52 ECMWF profile independent

set (Chevallier, 2000) for HIRS, ASMU-A and IASI. This tests the differences of the brightness temperatures simulated by RTTOV-10 with the new coefficients which should be small. Several viewing angles are computed.

- The transmittance profiles for RTTOV-10 and RTTOV-9 are compared for HIRS (v7 predictors 43L/51L), IASI (v9 predictors all gases 101L) and ASMU-A (v7 predictors 43L/51L) for the 52 profile set which is an independent set of profiles for the RTTOV-10 coefficients.

- The jacobians for RTTOV-10 and RTTOV-9 are compared for HIRS (v7 predictors 43L/51L), IASI (v9 predictors all gases 101L) and ASMU-A (v7 predictors 43L/51L) for the 52 profile set.

- Comparisons of RTTOV-9 and RTTOV-10 simulations with observations using the ECMWF IFS for many sensors including HIRS, AMSU and IASI.

The validation results described below are for ATOVS, IASI and AIRS but the performance of the new RTTOV-10 model for all other instruments is similar. In addition where changes have been made to the calculations for RTTOV-10 (e.g. Zeeman effect, FASTEM-4) then specific validation tests are made as described in the following sections or in the references provided in this report. ECMWF have also reported separately on their implementation of RTTOV-10 in their IFS (Bormann *et. al*.; 2011) and this is a useful document to refer to alongside this one.

4.1 Validation of top of atmosphere radiances

4.1.1 Comparison of simulations

The primary outputs from RTTOV are the top of atmosphere radiance for each channel and so this is the main parameter for which the RTTOV-10 simulations are checked and compared with the corresponding RTTOV-9 values. The main reason for differences between RTTOV-9 and RTTOV-10 computed radiances are due to the new line-by-line transmittances with more up to date spectroscopy, more layers on which the optical depth calculation is done and better treatment of the profile at the bottom and top. Comparisons between RTTOV-9 (v93) and RTTOV-10 (v1) were made according to the parameters listed in Table 4 for calculations on a 52 diverse profile set. The mean differences were then plotted in the following figures. For all the plots shown the blue bars are the actual difference between the recommended RTTOV-9 and RTTOV-10 coefficients.

The results are shown for NOAA-15 HIRS channels in Figure 2 using version 7 predictors throughout. The first comparison was to compare the effect of the increased number of levels from 43 to 51 for RTTOV-10 coefficients and this is shown by the red bars in Figure 2. As expected only the stratospheric channels and to a lesser extent the ozone and upper tropospheric water vapour channel show significant differences. The change to a new line-by-line radiative transfer model to compute the transmittances (see section 2.6.2) result in larger differences of up to 0.7K for HIRS channel 6 shown in blue. Note the other difference here will be the diverse profile dataset changing from the TIGR dataset to the ERA-40 diverse set. These results show that different biases will be seen in NWP systems when RTTOV-10 replaces RTTOV-9 and a retuning will be required.

Parameters	RTTOV-93	RTTOV-10
Number of layers for optical depth calculation	43 (0.1-1013hPa) except for IASI: 101 (0.005-1050hPa)	51 (0.005-1050hPa) except for IASI: 101 (0.005-1050hPa)
Input Profile set	52 Profiles on 43L	52 Profiles on 51L
Infrared Sensors		
Spectroscopic data	GENLN2/HITRAN-96	LBLRTMv11.1/ HITRAN2006/GEISA
Emissivity assumed	0.98	0.98
Optical depth predictors	Version 7 HIRS Version 9 IASI	Version 7 HIRS Version 9 IASI
Microwave Sensors		
Spectroscopic data	Liebe 89/92 Mean layer values	Liebe 89/92 Curtis-Godson
Emissivity assumed	0.6	0.6
Optical depth predictors	Version 7	Version 7

Table 4. The parameters assumed for the RTTOV-9 and RTTOV-10 comparisons

Figure 2. Difference in NOAA-15 HIRS brightness temperatures for RTTOV-93 and RTTOV-10 calculations with version 7 predictors. Blue shows the difference between 43L Genln2 and 51L LBLRTM coefficients and red uses the same LBL model and so shows only the effect of the different levels.

For NOAA-15 AMSU-A channels the results are shown in Figure 3 again using version 7 predictors. There are three comparisons in this case plotted. The first in blue show the

impact of the additional levels and the updated radiative transfer (see section 2.6.3) in the RTTOV-10 coefficient file and only the stratospheric channels are affected but there is a large change of up to 2K for AMSU channel 13. Previous studies have shown there were insufficient levels in the stratosphere to represent the vertical temperature structure and these results confirm this for AMSU-A. The green bars show the differences when the same layers are used in the calculation and only the radiative transfer is changed which results in about half of the overall bias. This is not only due to the new spectroscopy in the MW radiative transfer but also the different diverse profile datasets which are used for the line-by-line simulations. The purple bar attempts to quantify the impact of the different profile datasets used with same radiative transfer used for each profile set and the differences appear to be small between the 43L TIGR set and the 52L ERA set. It appears about half the difference between RTTOV-9 and RTTOV-10 simulations is due to the improved layering and the other half due to the improved radiative transfer.

For AMSU-B/MHS channels the differences are much smaller as shown in Figure 4 and the change in radiative transfer with the exception of channel 3 only has a small effect with most of the change due to the new levels. The changes outlined in section 2.6.3 contribute to these small changes in brightness temperature.
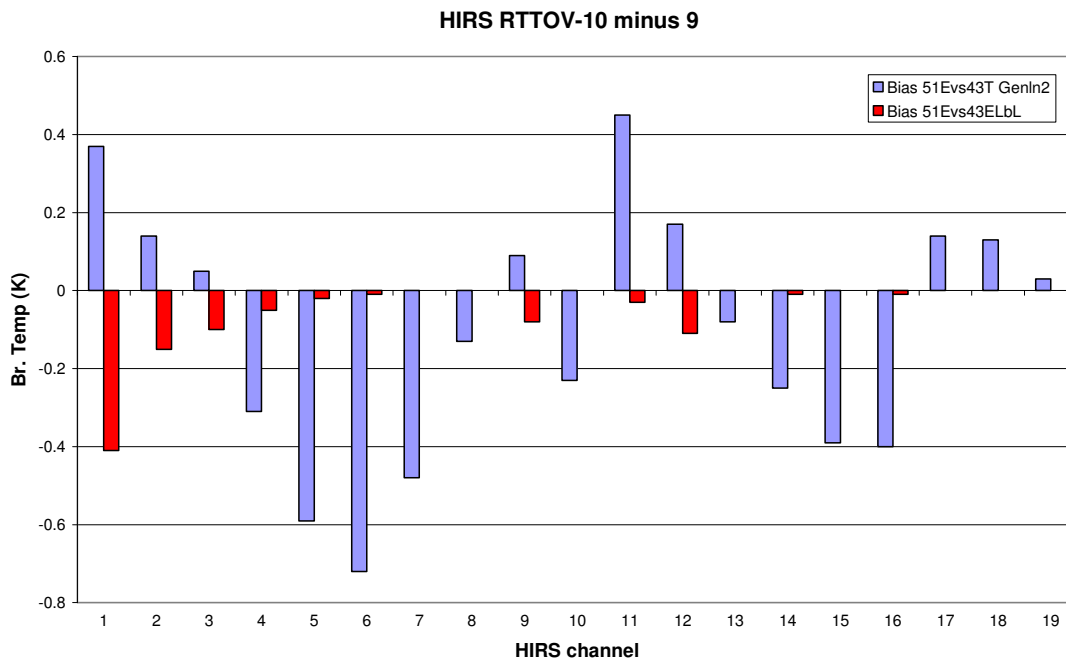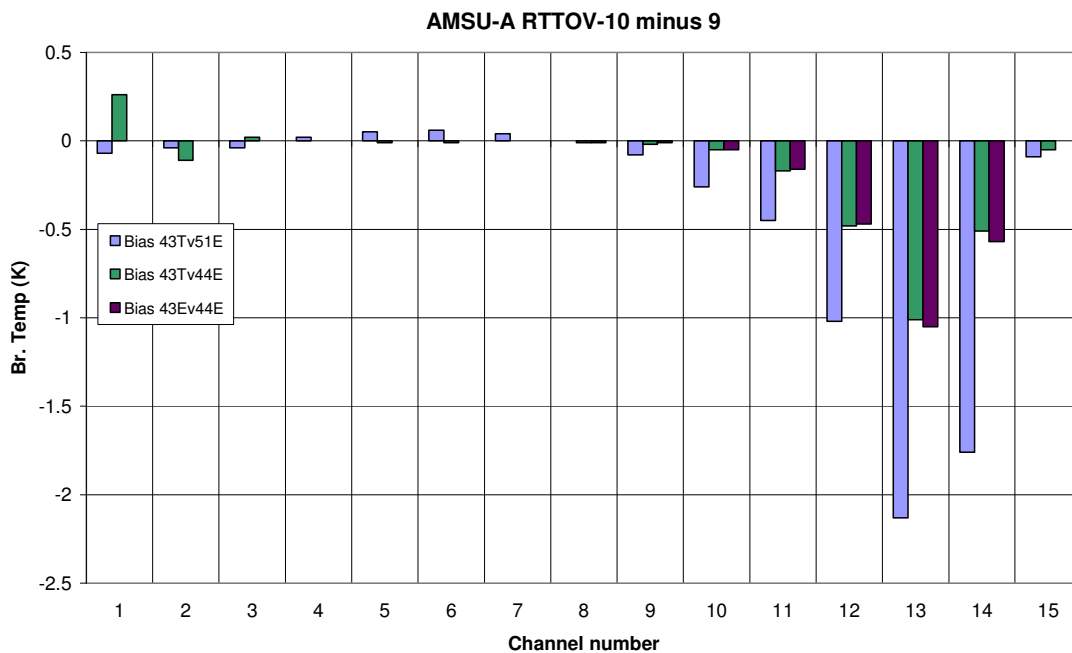

Figure 3 Difference in NOAA-15 AMSU-A brightness temperatures for RTTOV-93 and RTTOV-10 calculations with version 7 predictors. Blue shows the difference between the official RTTOV-9 and RTTOV-10 coefficients which includes different levels and new line-by-line references. The green bars show the same but the rttov coefficients are on 43L. The purple bars are where RTTOV-9 coefficients are computed using the new diverse profile set compared to RTTOV-10 coefficients.
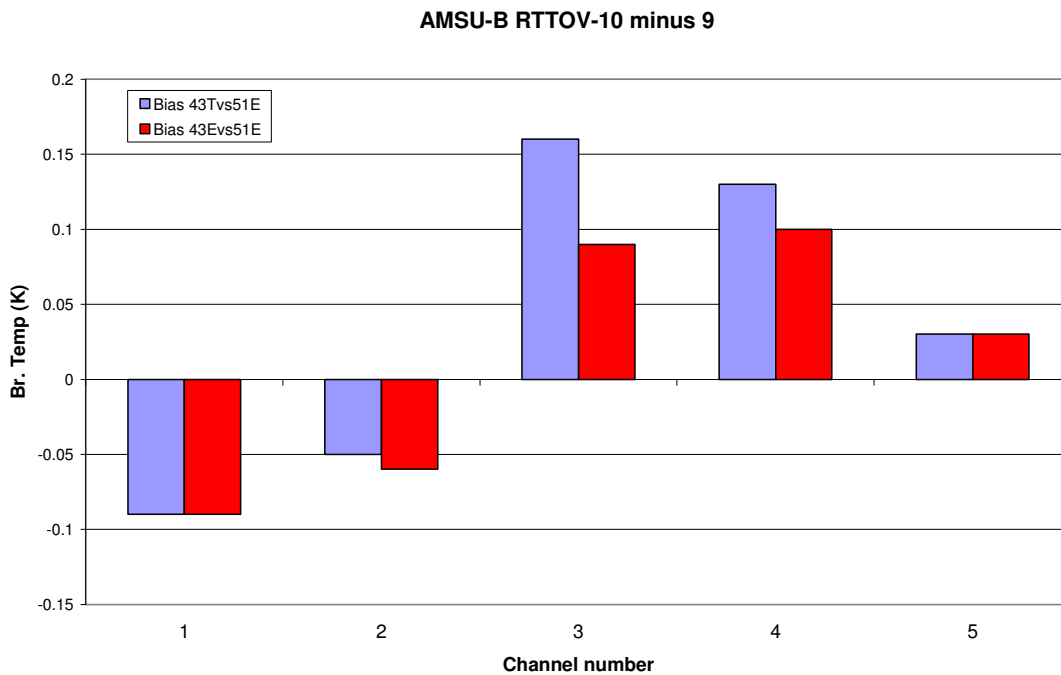
AMSU-B RTTOV-10 minus 9

Figure 4. Difference in NOAA-15 AMSU-B brightness temperatures for RTTOV-93 and RTTOV-10 calculations with version 7 predictors. Blue shows the difference between the official RTTOV-9 and RTTOV-10 coefficients which includes different levels and red shows where the same radiative transfer model is used for the RTTOV-9 coefficients.

A selection of IASI channel differences are shown in Figure 5 again only for version 7 predictors and so not including the trace gases. This time the bias and standard deviation of the difference is plotted. With the exception of the stratospheric channel (93 at 668cm^{-1}) all the differences are well below 0.5K. In this case the RTTOV-9 coefficient file is based on kCarta line-by-line model on 101L and the RTTOV-10 file on the LBLRTM model on 101L so the differences here are purely down to the new spectroscopy. The main difference is for the high peaking channel in the CO_2 $v2$ band where the CO_2 line mixing for example has changed and updated line parameters can also contribute to the differences.
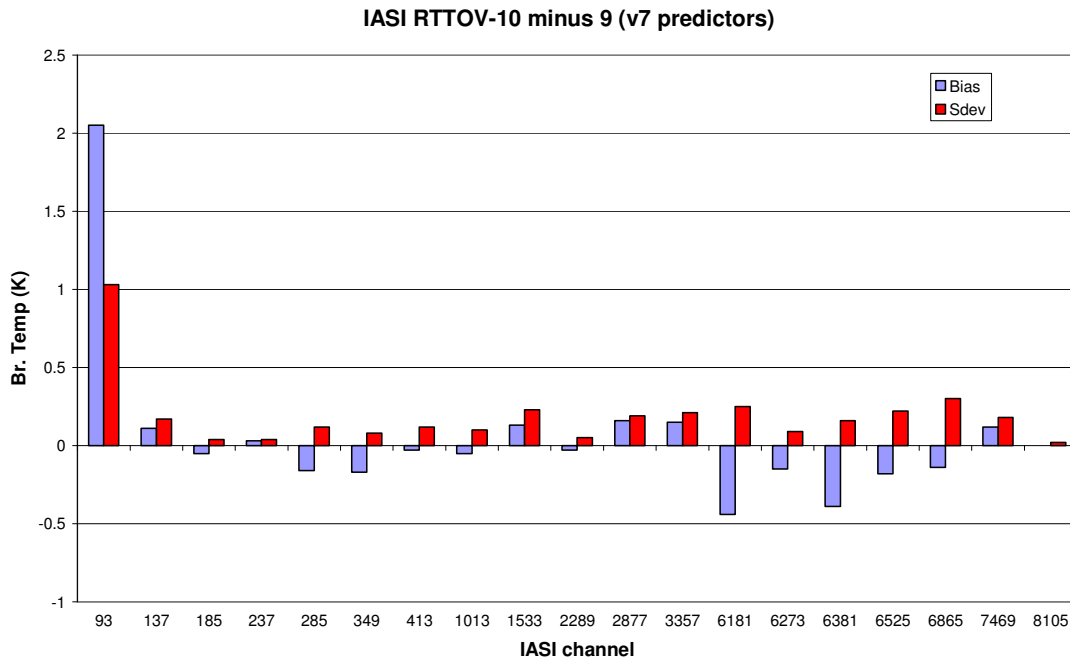
IASI RTTOV-10 minus 9 (v7 predictors)

Figure 5. Difference in METOP-A IASI brightness temperatures for RTTOV-93 and RTTOV-10 calculations with the mean (blue) and standard deviation (red) of the difference plotted. The RTTOV-9 coefficients are based on kCarta on 101L and the RTTOV-10 coefficients on LBLRTM on 101L.

4.1.2 Comparison with observations

A comparison of the RTTOV-9 and RTTOV-10 radiances with coincident observations is made using the ECMWF IFS model fields. The same coefficient files (RTTOV-10 files were just reformatted RTTOV-9 files) were used for this so unless there are bugs in the code the differences should be negligible. A one month run of the IS model from 15 May 2010 to 14 June 2010 was run with RTTOV-9 (control) and with RTTOV-10 (experiment) and the corresponding O-B and O-A statistics were collected for several different instruments. The same surface emissivities were used. Plots for AMSU-A and AIRS are shown in Figures 6 and 7 respectively. They show no significant differences between the runs with either version of RTTOV except the different treatment of the model top leads to many more observations being used for high peaking AIRS channels with RTTOV-10.
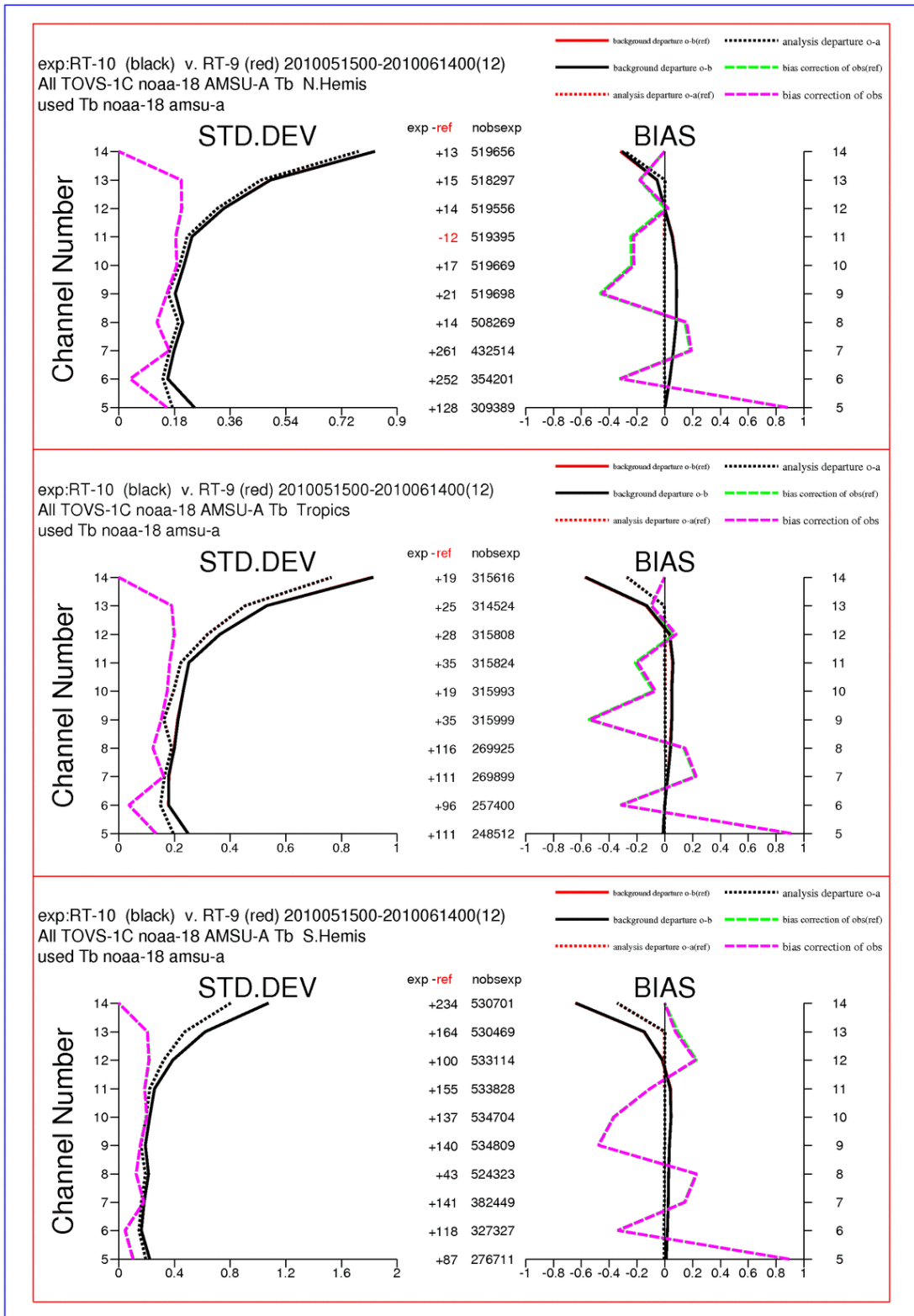
Figure 6. Comparison of METOP-A AMSU-A observed – simulated brightness temperatures for RTTOV-9 (red) and RTTOV-10 (black) in the ECMWF analysis.
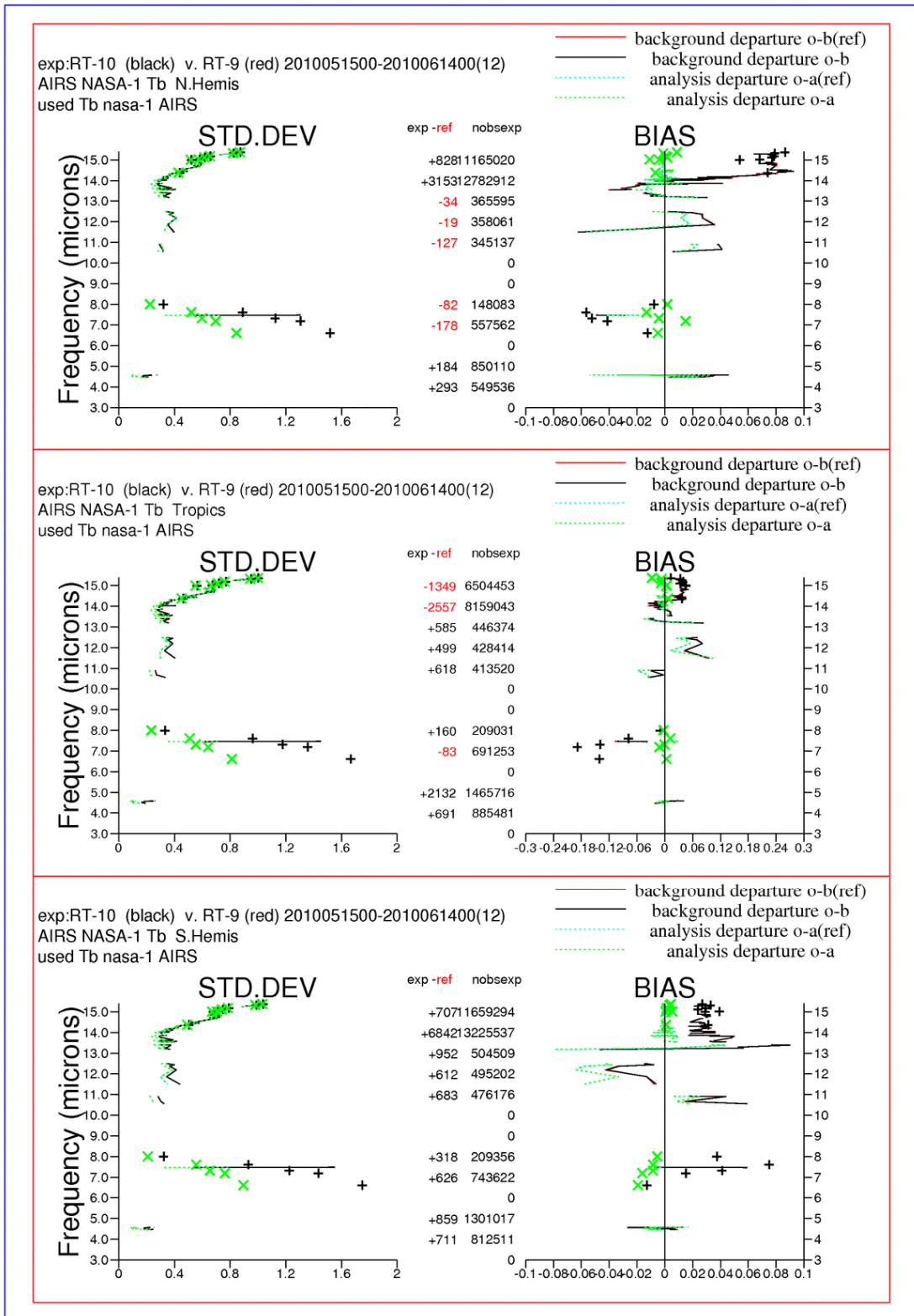
Figure 7. Comparison of AIRS observed – simulated brightness temperatures for RTTOV-9 (red) and RTTOV-10 (black) in the ECMWF analysis.

4.2 Comparison of jacobians

The accuracy of the jacobians computed by RTTOV is important to document for the radiance assimilation users as they are instrumental in modifying the NWP model analysis
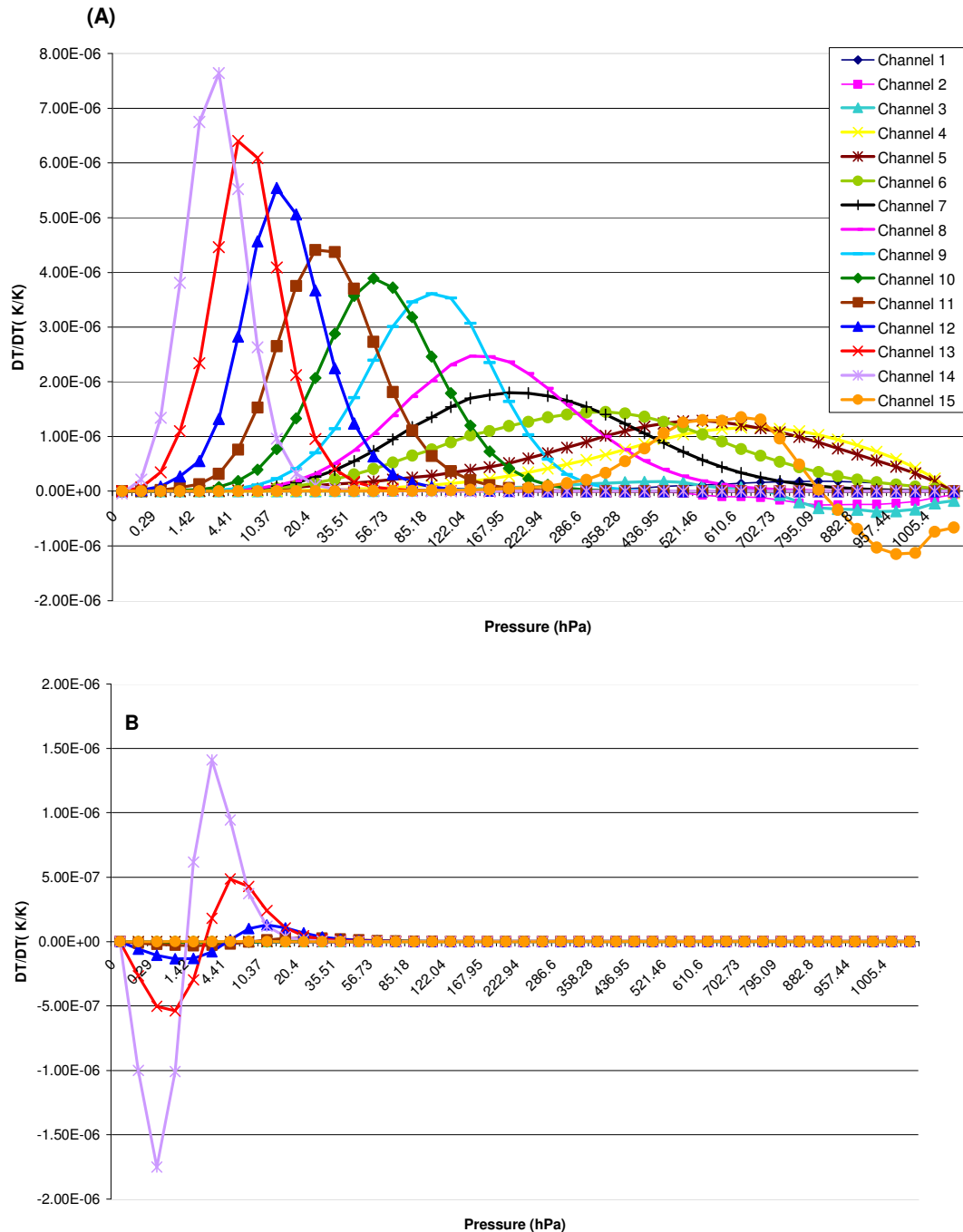
Figure 8. In the top panel (A) AMSUA-A temperature jacobians computed with RTTOV-10 on the 44 levels for all 15 channels for a moist tropical profile are plotted and the bottom panel (B) shows the mean differences from the equivalent RTTOV-9 calculation for a 52 diverse profile set.

variables. This section describes a comparison of the nadir view jacobians for AMSU-A channels generated by RTTOV-7 predictors with the RTTOV-9 and RTTOV-10 codes. The

temperature jacobians for a single moist tropical profile are plotted in Figure 8A. Computations were made for nadir views with FASTEM-3 used to define the surface emissivity for both RTTOV versions. The prescribed temperature perturbation was +1K. The mean difference between the RTTOV-10 and RTTOV-9 calculations for the 52 profile diverse set on 43L (RTTOV-9) and 44L (RTTOV-10) is shown in Figure 8B. With the exception of the high peaking channels the differences are zero at all levels. The differences for the high peaking channel are due to the different treatment of the top layer of the profile in RTTOV-10 (see section 2.6.1) compared to RTTOV-9 and these are significant for channel 14. For the water vapour jacobians no differences were seen as they are insensitive to changes at the profile top. The internal level interpolation is active for these tests but the differences are still seen when this is not used. It should be noted that the additional levels now in the RTTOV-10 coefficient files will also help to improve the jacobians especially in the stratosphere but it is difficult to compare jacobians on different layers.

4.3 Validation of IR emissivity atlas

The results of the validation of the IR emissivity atlas are outlined in Borbas et. al. (2011). In addition its use in the Met Office Autosat system for SEVIRI cloud detection has shown an improved ability to simulate the SEVIRI radiances over land. Clear-sky radiative transfer simulations are carried out using RTTOV-10 on recent NWP model forecast fields and the resulting radiances are used for cloud detection and in other derived cloud products. Figure 9 below shows histograms of observed minus simulated clear-sky radiances over land surfaces within the SEVIRI field of view at 00Z on 16 November 2009. Results for four key channels used in the processing (3.9, 8.7, 10.8 and 12.0 µm) are shown. (For the 3.9 µm channel only pixels with local solar zenith angle greater than 90° are included). The red lines show the default RTTOV case in which a fixed land surface emissivity of 0.98 is used.
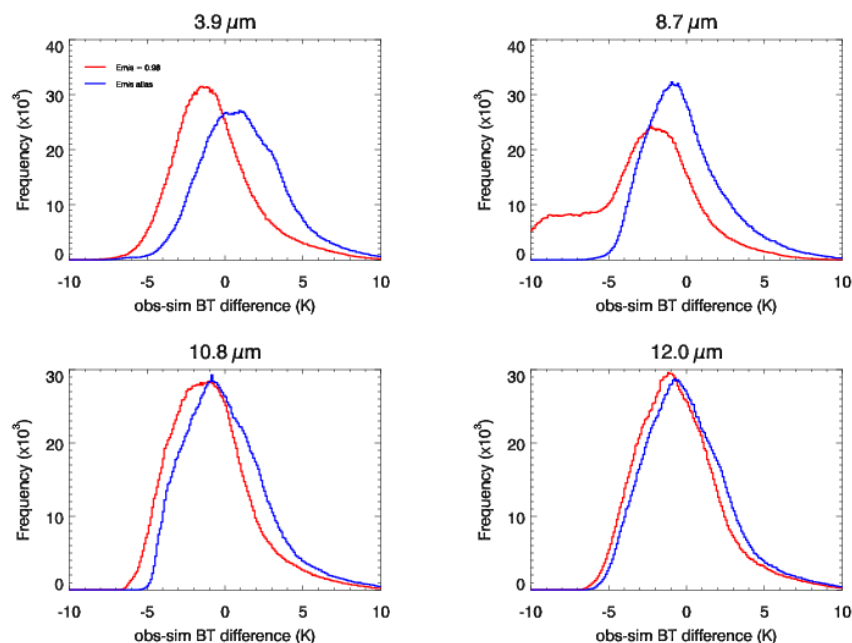

Figure 9. Observed minus simulated clear-sky brightness temperatures over land surfaces for four SEVIRI channels for the 00Z slot on 16 November 2009. In red, the RTTOV default fixed land surface emissivity of 0.98 was used, while in blue the RTTOV IR atlas was used.
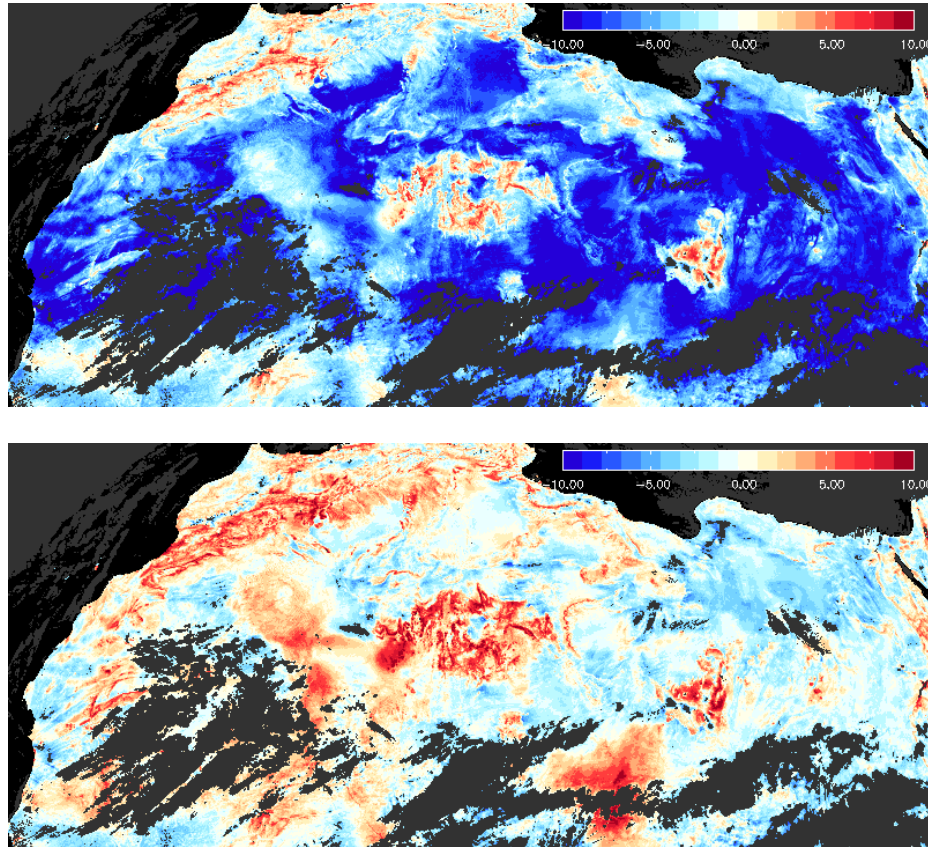
Figure 10. Observed minus simulated clear-sky brightness temperatures for the 8.7 μm SEVIRI channel over the Saharan region for the 00Z slot on 16 November 2009. In the top image, the fixed land surface emissivity of 0.98 was used. In the bottom image, the RTTOV IR atlas was used. Grey pixels are cloud-contaminated and black pixels are ocean.

	O-B	ch04	ch05	ch06	ch07	ch08	ch09	ch10	ch11
Fixed 0.98	Mean - day	-	-0.23	0.08	-3.08	5.33	-0.52	-0.24	-1.71
	StDv - day	-	2.34	2.03	4.72	2.78	3.84	3.78	2.24
	Mean - night	-0.76	-0.13	0.24	-3.01	4.93	-0.88	-0.49	-1.40
	StDv - night	2.56	2.30	1.76	3.44	2.03	2.55	2.59	1.47
IR atlas	Mean - day	-	-0.23	0.08	0.29	6.62	0.56	0.39	-1.47
	StDv - day	-	2.34	2.03	3.47	2.63	3.87	3.85	2.25
	Mean - night	1.07	-0.13	0.24	-0.09	6.00	0.08	0.06	-1.23
	StDv - night	2.79	2.30	1.76	2.58	1.95	2.67	2.68	1.48

Table 5. Means and standard deviations for observed minus simulated clear-sky brightness temperatures over land surfaces for all SEVIRI IR channels with a fixed emissivity and with the IR atlas.

The blue lines show the results when using the IR atlas. The largest impact is seen in the 8.7 µm channel over barren surfaces as shown in Figure 10 which compares the O-B values in this channel for the same slot for the default fixed emissivity and the IR atlas. Table 5 shows the means and standard deviations of the observed minus simulated clear-sky

brightness temperatures over land in each SEVIRI IR channel over all hourly slots from 00Z to 23Z on 16 November 2009.

4.4   Validation of MW emissivity atlas

The results of the validation of the microwave emissivity atlas are outlined in Aires *et. al.* (2011). Work is now underway to test the impact of the atlas emissivities in an NWP context at the Met Office.

4.5   Validation of Zeeman effect

The prediction scheme for Zeeman channels (19-22) for SSMIS and its validation against the base line by line model and measurements is documented in Han (2007) and Han et al. (2007).

A comparison of the implementation in RTTOV-10 with that based on Han (2007) is shown in Table 6, using the mean profile of the coefficient training set. Since the original prediction scheme has been retained, small departures from the Han values will have arisen only on account of unrelated developmental changes in the wider code.

		SSMIS				AMSU-A	
B (µT)	cos(B,k)	Ch19	Ch20	Ch21	Ch22	Ch14	
60	0.0	238.59	227.71	248.84	252.57	252.23 K	RT10
		238.44	227.68	248.71	252.62	252.27 K	Han
40	0.0	234.70	225.72	253.37	252.40	251.95 K	RT10
		234.57	225.61	253.29	252.44	251.99 K	Han
20	0.0	232.08	225.71	254.42	252.29	251.83 K	RT10
		231.93	225.40	254.35	252.33	251.86 K	Han

0	0.0	238.24	231.06	254.18	252.26	251.35 K	RT10

Table 6. Variation of RTTOV-10 brightness temperature with geomagnetic field (10 µT=0.1 gauss) for the mean profile of the 83 level Zeeman training set with a satellite zenith angle of 55°. For each field value, the first row refers to RTTOV-10 and the second to Han (2007). The bottom row shows the brightness temperatures for the same profile when the standard non-Zeeman coefficients are used.

As the magnitude and direction of the geomagnetic field are varied, the pattern of absorption in the Zeeman channels is altered through a shift in the weighting functions, resulting in a change in the brightness temperature that depends both on the atmospheric temperature profile and the disposition of the channel passbands. For this profile, Table 6 shows that the effect of changing the field magnitude is small in AMSU-A channel 14 and SSMIS channel 22, but it is much larger in SSMIS channel 19. The bottom row of the Table corresponds to the computed brightness temperatures with no Zeeman effect included.

Table 7 shows the effect of changing the orientation of the geomagnetic field for the same profile and radiation path as before. Again, it is small in AMSU-A channel 14 and SSMIS channel 22, but is much more significant, this time, in SSMIS channels 19 and 20.

B (µT)	cos(B,k)	SSMIS				AMSU-A	
		Ch19	Ch20	Ch21	Ch22	Ch14	
60	0.0	238.59	227.71	248.84	252.57	252.23 K	RT10
		238.44	227.68	248.71	252.62	252.27 K	Han
60	0.5	239.46	228.53	248.87	252.53	251.95 K	RT10
		239.31	228.48	248.73	252.57	251.99 K	Han
60	1.0	242.44	232.30	248.82	252.40	251.83 K	RT10
		242.29	232.17	248.67	252.44	251.86 K	Han

Table 7. Variation in RTTOV-10 brightness temperature using, as in Table 6, the mean profile of the 83 level training set with a satellite zenith angle of 55°. Here, however, the field is fixed (60 µT=0.6 gauss) and only its orientation is changed. For each angle considered, the first row refers to RTTOV-10 and the second to Han (2007).

4.6 Validation of PC computations for IASI

See Matricardi (2010) for a comprehensive description of the results of the validation of PC-RTTOV.

4.7 Validation of FASTEM-4/5

The main results for FASTEM-4 are documented in Liu *et. al.* (2010). Subsequently the brightness temperatures and emissivities over sea for AMSU/MHS and AMSR-E have been evaluated at ECMWF comparing FASTEM-2, 3, 4 and a new version 5 not available in the original release of RTTOV-10 but may be released in a future update. The results for AMSR-E are shown in Figure 11 which shows that FASTEM-4 has a quite different behaviour for the h-pol channels compared with earlier versions of FASTEM.

This is partly due to its treatment of the foam coverage for high wind speeds and in many respects gives lower biases in the IFS model than earlier versions for conical scanning radiometers. The wind speed dependence of the bias is also important to consider as shown in Figure 12. where above 15 m/s the biases for all channels diverge for FASTEM-2 and FASTEM-4 with the v-pol channels having a smaller bias but the h-pol biases being of a similar magnitude to FASTEM-2 but opposite sign. The reduced bias for most AMSR-E channels at low wind speeds is likely to be due to the improved roughness parametrisation for the sea surface. Users should note the significant change in radiance they will see with FASTEM-4 especially for high wind speeds.

For AMSU-A window channels the benefits of FASTEM-4 over FASTEM-3 are less clear with large differences for high wind speeds for all window channels. The results for AMSU-A are reported in Bormann *et. al.* (2011). As a result FASTEM-5 was developed (sec 2.2) to further improve the microwave sea surface emissivities for inclusion in the delta release RTTOV-10.2. The O-B statistics for FASTEM-5 showed clear benefits for cross-track microwave sounders (i.e. AMSU-A) but the benefits were less clear for microwave imagers (i.e. AMSR-E).
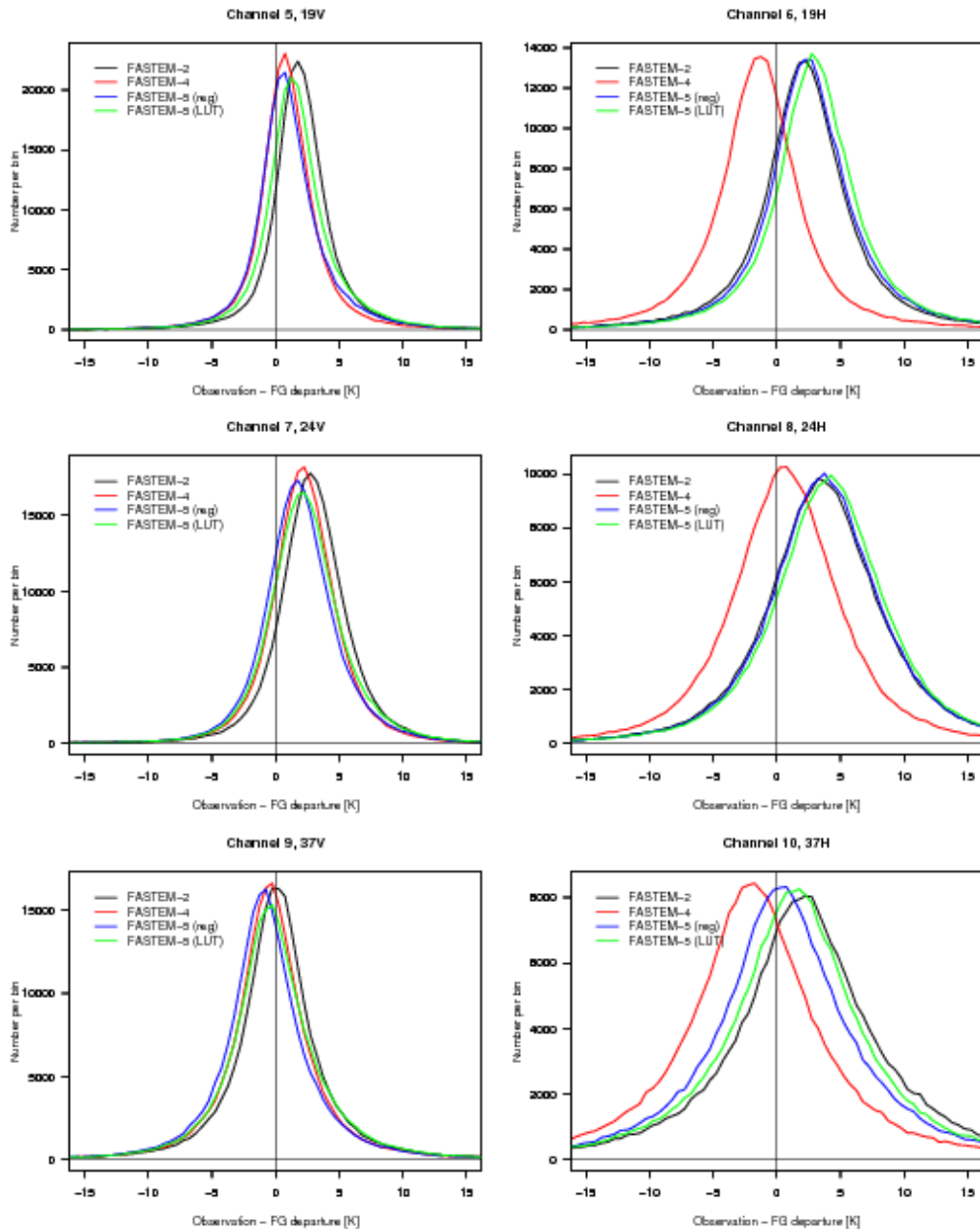
Figure 11. Comparison of different versions of FASTEM for ASMR-E channels in the ECMWF forecast system in terms of Ob-Fg for the period 5 -25 July 2010 .

4.8   Validation of microwave scattering code

There have been no significant changes to the science of the scattering code and so the normal tests made with code changes are considered to be sufficient for this release of RTTOV_SCATT but see section 3 and Geer *et. al.* (2009a) and Geer *et. al.* (2009b) for more details.
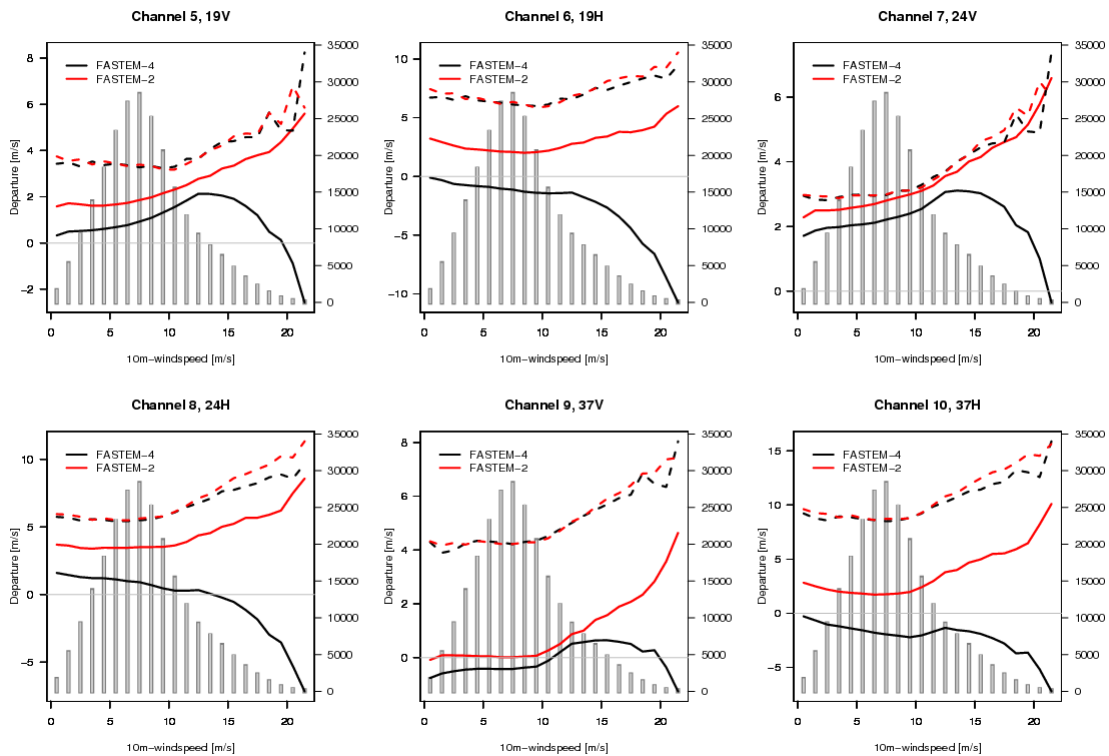
Figure 12. First guess departure statistics before bias correction for AMSR-E channels assimilated in the ECMWF system as a function of the model 10m wind speed for 5-25 July 2010 for all observations over ocean. The statistics are derived from experiments that actively assimilated AMSR-E observations using FASTEM-4 (black) or FASTEM-2 (red) respectively with biases (Ob-Fg) displayed in solid lines and st. dev. in dashed lines. Also shown in grey is the population of the data considered in the statistics (right hand y-axis).

5 Summary

The latest version of RTTOV, RTTOV-10 has been validated in several ways to show the same or improved performance for the prediction of satellite top of atmosphere radiances both for clear air, cloudy, aerosol and precipitating profiles. It builds on previous versions of RTTOV. The changes have been validated as described in this document and the references given. Referring to the list of changes made between RTTOV-9 and RTTOV-10 given in section 2 the following comments can be made:

Infrared and Microwave land surface emissivity atlases included as an option for improved simulations of window channels over land

Several studies have shown improved simulations of both infrared and microwave window channels over land especially for channels such as at 8.7µm where the emissivity is far from 0.98 the previous default value in RTTOV-9.

Improved Microwave emissivities over ocean using FASTEM-4/5 for low frequency channels

Studies at ECMWF and NCEP have shown improved fits of AMSR-E radiances over the ocean using FASTEM-4. For cross-track sounders FASTEM-5 gives better results.

Computation of principal components of radiances for IASI and AIRS

PC-RTTOV is being successfully used at ECMWF to enable the assimilation of clear sky PCs of the IASI shortwave band.

Inclusion of explicit treatment of the Zeeman effect for AMSU-A channel 14 and SSMIS channels 19-22.

Environment Canada has been doing simulations with the new treatment of the Zeeman effect. New space weather applications will also benefit from this improved simulation capability.

Improvements to treatment of top layer of user input profile

ECMWF demonstrate in Bormann et al (2011) that the better treatment of the top layer leads to improvements.

Updated IR sensor coefficients based on latest spectroscopy using LBLRTMv11 and updated MW sensor coefficients with improved atmospheric layering

Use of more recent spectroscopy has changed the simulated radiances for some IR and MW channels which should provide reduced biases to correct in NWP systems. This has been clearly seen for SSU simulations (P. Poli personal communication).

The number of layers for the optical depth calculation has increased from 43 to 51 for IR and MW radiometers

Evidence of improved simulations in the stratosphere with the enhanced number of levels. More needs to be done in assimilation mode to demonstrate this.

Improvements to microwave scattering code
Studies at ECMWF have optimised the code so it is up to 30% faster for simulating precipitation affected microwave radiances with no significant change in performance.

6 Acknowledgements

7 References

Aires, F., Prigent, C., Bernardo, F., Jiménez, C., Saunders, R. and Brunel, P. 2011 A Tool to Estimate Land-Surface Emissivities at Microwave frequencies (TELSEM) for use in numerical weather prediction. *Quart. J. Roy. Meteorol. Soc.,* **137***: 690–699. doi: 10.1002/qj.*

Bauer, P., E. Moreau, F. Chevallier, U. O'Keeffe, 2006: Multiple-scattering microwave radiative transfer for data assimilation applications, *Quart. J. Roy. Meteorol. Soc.*, **132**, *1259-1281*

Borbas, E.E., R. O. Knuteson, S. W. Seemann, E. Weisz, L. Moy, and H.-L. Huang, 2007: A high spectral resolution global land surface infrared emissivity database. *Joint 2007 EUMETSAT Meteorological Satellite Conference and the 15th Satellite Meteorology & Oceanography Conference of the American Meteorological Society, Amsterdam, The Netherlands, 24-28 September 2007. Available at:*

http://www.ssec.wisc.edu/meetings/jointsatmet2007/pdf/borbas_emissivity_database.pdf

Borbas, E.E, B.C. Ruston, R.O. Knuteson, and R.W. Saunders. 2011 Development of a MODIS-based Infrared Land Surface Emissivity Software Package for application to simulate satellite radiances: the RTTOV UWiremis Module, (*submitted to JGR).*

Bormann, N., A. Geer and T. Wilhelmsson 2011 Operational implementation of RTTOV-10 in the IFS. *ECMWF Tech. Memo. 650. http://www.ecmwf.int/publications/library/do/references/list/14*

Chevallier F, Di Michele S, McNally AP. 2006. 'Diverse profile datasets from the ECMWF 91-level short-range forecasts'. *NWP SAF Report No. NWPSAF-EC-TR-010.*

Clough, S. A., Shephard, M. W., Mlawer, E. J., Delamere, J. S., Iacono, M. J., Cady-Pereira, K., 25 Boukabara, S., and Brown, R. D. 2005 Atmospheric radiative transfer modeling: a summary of the AER codes., *J. Quant. Spectrosc. Ra*., **91**, *233–244*

Durden, S. P., and J. F. Vesecky 1985, A physical radar cross-section model for a wind-driven sea with swell, *IEEE J. Oceanic Eng.*, **OE-10**, *445–451*.

Eyre J.R. and H.M. Woolf 1988: Transmittance of atmospheric gases in the microwave region: a fast model. *Applied Optics* **27** *3244-3249*

Eyre J.R. 1991: A fast radiative transfer model for satellite sounding systems. *ECMWF Research Dept. Tech. Memo.* **176** *Available at http://www.ecmwf.int/publications/library/ecpublications/_pdf/tm/001-300/tm176.pdf*

Geer A.J., P. Bauer, and C.W. O'Dell,, 2009a: A revised cloud overlap scheme for fast microwave radiative transfer in rain and cloud, *J. App. Met. Clim.*, **48**, *2257–2270,*

Geer, A.J., R.M. Forbes and P. Bauer,, 2009b: Cloud and precipitation overlap in simplified scattering radiative transfer, *EUMETSAT/ECMWF Fellowship Programme Research Report no. 18,, available from www.ecmwf.int*

Han, Y., 2007: Incorporation of the JCSDA Zeeman RT model in RTTOV-9, *NWP SAF Visiting Scientist Report, available from the Met Office.*

Han, Y., F. Weng, Q. Liu and P. van Delst, 2007: A fast radiative transfer model for SSMIS upper atmosphere sounding channels, *J.Geophys.Res.*, **112**, *D11121, 12pp.*

Jacquinet-Husson N, Scott NA, Chedin A, Garceran K, Armante R, Chursin AA, Barbe A, Birk M, Brown LR, Camy-Peyret C, Claveau C, Clerbaux C, Coheur PF, Dana V, Daumont L, Debacker-Barilly MR, Flaud JM, Goldman A, Hamdouni A, Hess M, Jacquemart D, Kopke P, Mandin J-Y, Massie S, Mikhailenko S, Nemtchinov V, Nikitin A, Newnham D, Perrin A, Perevalov VI, Regalia-Jarlot L, Rublev A, Schreier F, Schult I, Smith KM, Tashkun SA, Teffo JL, Toth RA,Tyuterev VlG, Vander Auwera J, Varanasi P, Wagner G. 2005. The 2003 edition of the GEISA/IASI spectroscopic database. *J. Quant. Spectrosc. Radiat. Transfer*, **95**: 429-467.

Karbou, F., E. Gérard, F. Rabier, 2010, Global 4D-Var assimilation and forecast experiments using AMSU observations over land. Part-I : Impact of various land surface emissivity parameterizations, *Weather and Forecasting,* **25***, 5-19, doi : 10.1175/2009WAF2222243.1*

Karbou, F., E. Gérard, and F. Rabier, 2006, Microwave land emissivity and skin temperature for AMSU-A and -B assimilation over land, *Q. J. R. Meteorol. Soc.* **132***, No. 620, Part A, pp. 2333-2355(23), doi : 10.1256/qj.05.216*

Kobayashi S., M. Matricardi , A. McNally, D. Dee and S. Uppala. 2007: Recalculation of RTTOV coefficients for AMSU-A. *ECMWF Research Department Memorandum R43.7/SK/0763*

Kobayashi S., M. Matricardi , D. Dee and S. Uppala. 2008: Use of SSU and AMSU-A observations in reanalyses. *Extended abstract in 3rd WCRP International Conference on Reanalysis Tokyo 28 Jan – 1 Feb 2008. See http://wcrp.ipsl.jussieu.fr/Workshops/Reanalysis2008/abstract.html*

Kobayashi, S., Matricardi, M., Dee, D. and S. Uppala. 2009 Toward a consistent reanalysis of the upper stratosphere based on radiance measurements from SSU and AMSU-A. *Quarterly Journal of the Royal Meteorological Society* **135**, 2086–2099.

Koenig, M and E de Coning. 2009 The MSG Global Instability Indices Product and its Use as a Nowcasting Tool. *Weather and Forecasting:* **24***(1) 272.*

Liu, Q., F. Weng and S.J. English 2010 An improved fast microwave water emissivity model. *IEEE TGRS,* **49***, 1238 -1250.*

Matricardi, M and Saunders, R.W. 1999: A fast radiative transfer model for simulation of IASI radiances. *Applied Optics,* **38***, 5679-5691.*

Matricardi, M., Chevallier F, Kelly G, Thepaut J-N 2004: An improved general fast radiative transfer model for the assimilation of radiance observations. *Q. J. Roy. Meteorol. Soc.* **130** *153-173*

Matricardi, M., 2005: The inclusion of aerosols and clouds in RTIASI, the ECMWF fast radiative transfer model for the Infrared Atmospheric Sounding Interferometer. *ECMWF Technical Memorandum* **474** *(available at: http:/www.ecmwf.int/publications/library/references/list/14)*

Matricardi M. 2007. 'An inter-comparison of line-by-line radiative transfer models'. *ECMWF Technical Memo No. 525. European Centre for Medium-Range Weather Forecasts: Reading, UK. Available at http://www.ecmwf.int/publications/.*

Matricardi, M. 2008: The generation of RTTOV regression coefficients for IASI and AIRS using a new profile training set and a new line-by-line database. *ECMWF Research Dept. Tech. Memo.* **564.** *(available at: http://www.ecmwf.int/publications/library/do/references/list/14)*

Matricardi, M. and A. McNally 2008: An assessment of the accuracy of the RTTOV fast radiative transfer model using IASI data. *Proceedings of ITSC-16, Angra dos Reis, Brazil 7-13 May 2008.*

Matricardi, M. 2009: Technical Note: An assessment of the accuracy of the RTTOV fast radiative transfer model using IASI data. *Atmospheric Chemistry and Physics,* **9***, 6899-6913.*

Matricardi, M. 2010a: A principal component based version of the RTTOV fast radiative transfer model. *ECMWF Technical Memorandum 617 (available at: http:/www.ecmwf.int/publications/library/references/list/14)*

Matricardi, M. 2010b: A principal component based version of the RTTOV fast radiative transfer model. *Quarterly Journal of the Royal Meteorological Society,* **136***: 1823–1835. doi: 10.1002/qj.680*

Prigent C., W. B. Rossow, E. Matthews, 1997 Microwave land surface emissivities estimated from SSM/I observations, *Journal of Geophysical Research,* **102***, 21867-21890.*

Prigent, C., F. Aires, and W.B. Rossow 2006 Land Surface Microwave Emissivities over the Globe for a Decade. *Bulletin of the American Meteorological Society*, *DOI:10.1175/BAMS-87-11-1573, pp. 1572-1584.*

Prigent, C., E. Jaumouille, F. Chevallier, and F. Aires, 2008 A parameterization of the microwave land surface emissivity between 19 and 100 GHz, anchored to satellite-derived estimates, *IEEE Transaction on Geoscience and Remote Sensing ,* **46***, 344-352.*

Rosenkranz, P. W. and D. H. Staelin (1988), Polarized thermal microwave emission from oxygen in the mesosphere, *Radio Science,* **23***, 721-729.*

Rothman LS, Barbe A, Chris Benner D, Brown LR, Camy-Peyret C, Carleer MR , Chance K, Clerbaux C, Dana V, Devi VM, Fayt A, Flaud J-M, Gamache RR, Goldman A, Jacquemart D, Jucks KW, Lafferty WJ, Mandin J-Y, Massie ST, Nemtchinov V, Newnham DA, Perrin A, Rinsland CP, Schroeder J, Smith KM, Smith MAH, Tang K, Toth RA, Vander Auwera J, Varanasi P, Yoshino K. 2003. The HITRAN molecular spectroscopic database: edition of 2000 including updates through 2001. *J. Quant. Spectrosc. Radiat. Transfer*, **82:** *5-44.*

Rothman LS, Jacquemart D, Barbe A, Chris Benner D, Birk M, Brown LR, Carleer MR, Chackerian Jr. C, Chance K, Coudert LH, Dana V, Devi VM, Flaud J-M, Gamache RR, Goldman A, Hartmann J-M, Jucks K.W., Maki AG, Mandin J-Y, Massie ST, Orphal J, Perrin A, Rinsland CP, Smith MAH, Tennyson J, Tolchenov RN, Toth RA, Vander Auwera J, Varanasi P, Wagner G. 2005. The HITRAN 2004 molecular spectroscopic database. *J. Quant. Spectrosc. Radiat. Transfer*, **96** *139-204*.

R7REP2002 RTTOV-7 science and validation report available at:
http://research.metoffice.gov.uk/research/interproj/nwpsaf/rtm/rttov7_svr.pdf

R8REP2006 RTTOV-8 science and validation report available at:
http://research.metoffice.gov.uk/research/interproj/nwpsaf/rtm/rttov8_svr.pdf

R9REP2008 RTTOV-9 science and validation report available at:
http://research.metoffice.gov.uk/research/interproj/nwpsaf/rtm/rttov9_files/rttov9_svr.pdf

Saunders R.W., M. Matricardi and P. Brunel 1999a: A fast radiative transfer model for assimilation of satellite radiance observations - RTTOV-5. *ECMWF Research Dept. Tech. Memo.* **282** *(available from http://www.ecmwf.int/publications/library/do/references/list/14).*

Saunders R.W., M. Matricardi and P. Brunel 1999b: An Improved Fast Radiative Transfer Model for Assimilation of Satellite Radiance Observations. *Q. J. Roy. Meteorol. Soc. ,* **125,** *1407-1425.*

Seeman, S.W., Borbas, E.E., Knuteson, R.O., Stephenson, G.R. and Huang, H-L. 2008: Development of a global infrared emissivity database for application to clear sky sounding retrievals from multi-spectral satellite radiances measurements. *J. Appl. Meteorol. and Clim.* **47** *108-123.*

End of Report